

Article

High Degree of Differentiation and Enrichment of Li, Rb and Cs in Potassic-Ultrapotassic Volcanic Rocks: An Example from the Lhasa Block, Tibet

Dong Che ¹, Mianping Zheng ^{1,*}, Yuanyi Zhao ¹, Zhaozhi Zhang ^{1,2}, Chuanyong Ye ¹, Enyuan Xing ¹, Xuefei Zhang ¹ and Mingming Li ³

¹ MNR Key Laboratory of Saline Lake Resources and Environments, Institute of Mineral Resources, Chinese Academy of Geological Sciences, Beijing 100037, China

² Salt Lake Group of Qinghai, Golmud 816000, China

³ College of Geoscience and Surveying Engineering, China University of Mining and Technology (Beijing), Beijing 100083, China

* Correspondence: zhengmp2010@126.com

Abstract: Post-collisional potassic-ultrapotassic volcanic rocks are widely developed in the Lhasa block, Qinghai-Tibet region. In this paper, it was observed for the first time that dilute alkali elements—Li, Rb, and Cs—exhibit supernormal enrichment in the research data of numerous potassic-ultrapotassic volcanic rocks in the Lhasa block. At the same time, there are few studies on the genesis of enrichment. Currently, 568 sets of published volcanic rock data and 8 sets of measured data in the Lhasa block are sorted in detail, and the genesis of dilute alkali element enrichment is explained by means of geochemical research methods. It is believed that the high degree of magmatic fractionation of potassic-ultrapotassic volcanic rocks in the Lhasa block is the main reason for the abnormal enrichment of dilute alkali elements such as Li, Rb, and Cs. The abnormal enrichment area is mainly located in the central and western parts of the Lhasa block with an age range of 25–13 Ma. The discrimination range of Zr/Hf and Nb/Ta with a high degree of differentiation of potassic-ultrapotassic volcanic rocks in the Lhasa block is divided by analogy with the research results of highly fractionated granites, which provides a reference for the study of the supernormal enrichment of dilute alkali elements in potassic-ultrapotassic volcanic rocks in this area.

Keywords: Lhasa block; potassic-ultrapotassic volcanic rocks; alkali-rich; highly fractionated; Tibet



Citation: Che, D.; Zheng, M.; Zhao, Y.; Zhang, Z.; Ye, C.; Xing, E.; Zhang, X.; Li, M. High Degree of Differentiation and Enrichment of Li, Rb and Cs in Potassic-Ultrapotassic Volcanic Rocks: An Example from the Lhasa Block, Tibet. *Minerals* **2023**, *13*, 342. <https://doi.org/10.3390/min13030342>

Academic Editor: Ilya Bindeman

Received: 23 January 2023

Revised: 17 February 2023

Accepted: 26 February 2023

Published: 28 February 2023



Copyright: © 2023 by the authors. Licensee MDPI, Basel, Switzerland. This article is an open access article distributed under the terms and conditions of the Creative Commons Attribution (CC BY) license (<https://creativecommons.org/licenses/by/4.0/>).

1. Introduction

Since the post-collision of the Lhasa block in the Qinghai-Tibet Plateau, potassic-ultrapotassic volcanic rocks have been widely developed. Many scholars have conducted in-depth research on the volcanic rocks in this area for decades with respect to formation age, tectonic background, and source area properties [1–10], and much progress has been made. For example, potassium-rich volcanic rocks in the Majiang area of the Lhasa block are produced in an extensional tectonic environment [1]. The formation of post-collisional ultrapotassic rocks in southern Tibet is related to the convective thinning of thickened lithospheric mantle [11]. The post-collisional potassic intermediate-acid volcanic rocks in the Xiongba area originated from the partial melting of the crust [3]. The spatial distribution of post-collisional magmatism is controlled by east-west-oriented extensional tectonics [4,10]. Convection thinning/delamination occurred at the bottom of the thickened lithospheric mantle during the post-collision stage (25–10 Ma) [10]. Some potassic intermediate-acid volcanic rocks have the geochemical characteristics of adakite and contain subducted Indian continental crustal material [12] (Figure 1).

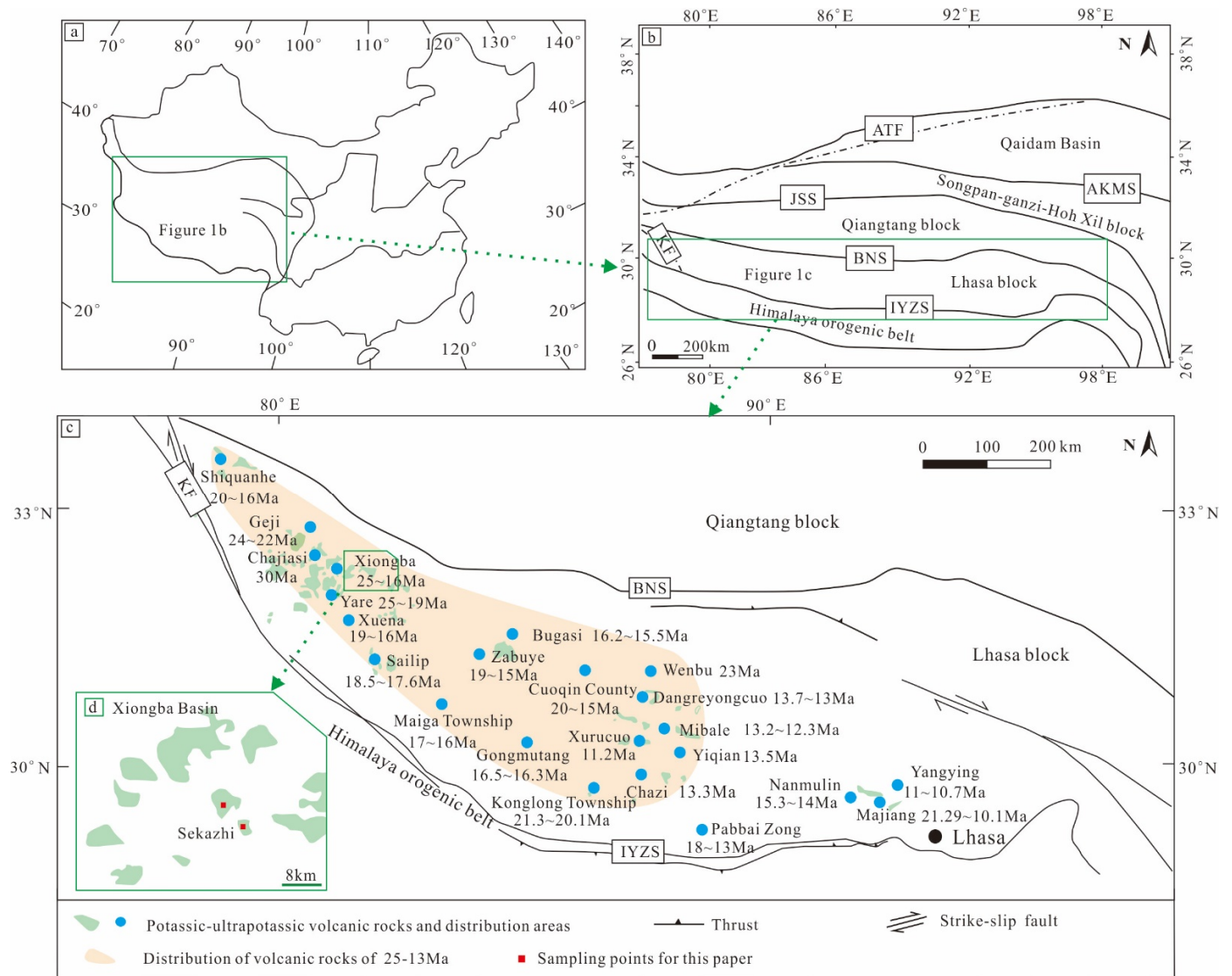


Figure 1. (a) Location map of the Qinghai-Tibet Plateau in China. (b) Location map of the study area in the Qinghai-Tibet Plateau. (c) Distribution map of potassic-ultrapotassic volcanic rocks and age since post-collision in the Lhasa block (modified from [4,9,10]). (d) Location map of Sekazhi. The source of age data is the same as that in Table 1. AKMS: Anymaqen-Kunlun-Muz-tagh suture zone; JSS: Jinshajiang suture zone; KF: Karakoram fault; BNS: Bangong-Nujiang suture zone; IYZS: Yaluzangbu suture belt; ATF: Altai left-lateral strike-slip fault.

Studies on the enrichment of Li, Rb, and Cs in rocks consider highly differentiated granites and pegmatites as the main carriers, and these studies use $Zr/Hf < 38$ and $Nb/Ta < 17$ as the main markers for distinguishing highly differentiated granites [13]. In a study of the differentiation of granitic gneisses with high Li, Rb, and Cs enrichment, it was concluded that Nb-Ta-rich granitic gneisses segregate to a higher degree of crystallization and that the granitic melt changes from being potassium-rich to sodium-rich when $Zr/Hf = 20$ [14]. The characteristics of high silicon, rich alkali, low magnesium, low titanium, and the enrichment of LREE and LILE in trachyte may indicate that rocks have undergone a high degree of evolution [15].

The anomalous enrichment of Li, Rb, and Cs exists in potassic-ultrapotassic volcanic rocks in the Xiongba Basin, which is located in the western part of the Lhasa block [16]. Combined with the unique characteristics of the enrichment of Cs and Rb in the salt lakes of the Lhasa block, it is speculated whether the potassic-ultrapotassic volcanic rocks in the

entire Lhasa block also have the anomalously enriched dilute alkali elements. Currently, not only are there few studies on the supernormal enrichment of Li, Rb, and Cs and crystallization differentiation degree in potassic-ultrapotassic volcanic rocks since the post-collision of the Lhasa block, but the relationship between the two has also never been discussed. In this paper, the causes of the supernormal enrichment of dilute alkali elements and the volcanic rocks' differentiation degree are discussed by analyzing the data of many volcanic rocks in this area.

2. Distribution and Characteristics of Potassic-Ultrapotassic Volcanic Rocks in the Lhasa Block

The rock types of post-collisional magmatism on the Qinghai-Tibetan Plateau are diverse and widely distributed in the Lhasa block in southern Tibet [1–8]. During the post-collisional tectonic-magmatic evolution stage of southern Tibet, the Oligocene-Miocene potassic-ultrapotassic volcanic rocks occurred in an east-west extensional setting in the Lhasa block. As the magmatic products of geodynamic processes at depths, post-collisional magmatism offers an opportunity to investigate the geodynamic processes responsible for plateau uplift [1,10]. Under the background of the continuous northward subduction of the Indian continental lithosphere, the Lhasa block in southern Tibet mainly develops three types of post-collision magmatic rocks: ultrapotassic rocks, potassic intermediate-acid volcanic rocks, and adakitic rocks [1,3,10].

The potassic-ultrapotassic volcanic rocks in the Lhasa block are mainly distributed in Shiquanhe, Geji, Chajiasi, Yare, Xiongba, Xuena, Sailip, Maiga Township, Zabuye, Bugasi, Konglong Township, Gongmutang, Cuoqin County, Xurucuo, Dangreyongcuo, Wenbu, Chazi, Yiqian, Mibale, Pabbai zong, Nanmulin, Majiang, Yangying, and other areas (Figure 1c). The ultrapotassic volcanic rocks in the Lhasa block of southern Tibet are mainly trachyandesite, basaltic trachyandesite, and alkali basaltic rocks produced in the form of volcanic lavas. The main lithology of potassic volcanic rocks includes trachyte, trachydacite, dacite, and rhyolite (Figure 2) [10].

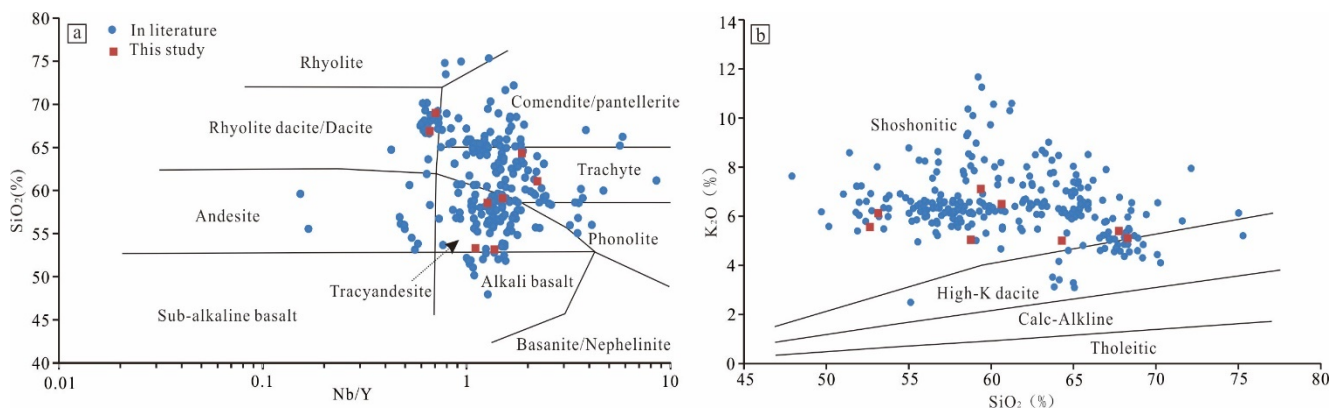


Figure 2. The diagrams of potassic-ultrapotassic volcanic rocks in the Lhasa block: (a) Nb/Y versus SiO₂ diagram (after Winchester and Floyd [17]); (b) SiO₂ versus K₂O diagram (after Peccerillo and Taylor [18]). The source of data is the same as that in Table 1.

In the porphyritic structure of potassic-ultrapotassic volcanic rocks in the Lhasa block, the proportion of phenocrysts is about 10%–20%, and phenocryst minerals include K-feldspar, plagioclase, diopside, amphibole, biotite, pyroxene, olivine, phlogopite, etc. (Figure 3a–f); the above phenocryst assemblage shows that magmatic crystallization differentiation is widespread. The matrix exhibits rough structures, trachytic texture, and cryptocrystalline structure, and the composition is the same as the phenocrysts [19,20].

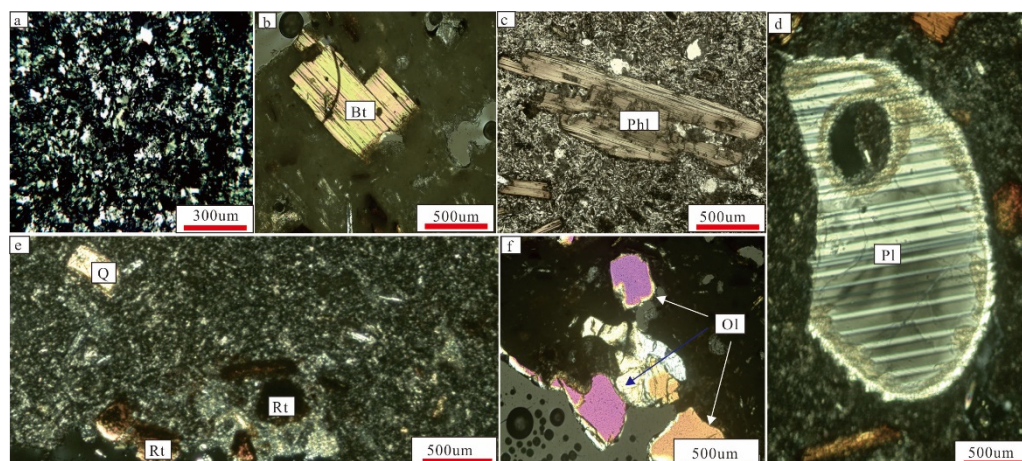


Figure 3. Microscopic structure images of potassic-ultrapotassic volcanic rocks in the Xiongba area. (a)—rhyolite; (b)—trachyte; (c–f)—trachyandesite; Bt = biotite; Q = quartz; Phl = phlogopite; Rt = rutile; Ol = olivine; Pl = plagioclase.3. Statistics of Li, Rb, and Cs Contents in Volcanic Rocks.

In this paper, the measured samples for the analysis of major, trace, and rare earth elements comprise eight potassic-ultrapotassic volcanic rocks in the Sekazhi area of the Xiongba Basin (Figure 1d), including trachyandesite (SKZ-J-1, SKZ-J-2, SKZ-J-3, and SKZ-J-4), trachyte (SKZ-J-5 and SKZ-J-6), rhyolite dacite (SKZ-J-7 and SKZ-J-8) (Appendix A). Whole-rock analyses of major and trace elements were conducted at the Institute of Beijing Research Institute of Uranium Geology, Beijing, China. Major element oxides were determined using an X-ray fluorescence spectrometer (XRF), with analytical precision being better than $\pm 2\text{--}5\%$. Trace elements were determined using PerkinElmer ICP-MS, with analytical precision being better than $\pm 5\%$ for most elements. Reference data sources of Li, Rb, and Cs are shown in Table 1.

Table 1. Reference data sources for potassic-ultrapotassic volcanic rocks in the Lhasa block (Li, Rb, and Cs ppm).

Scheme.	Distribution of Volcanic Rock	Age (Ma)	Average Content (ppm) and Numbers (n)			References
			Li	Rb	Cs	
1	Shiquanhe	20~16	—	425.51 (n = 5)	—	[21]
2	Geji	24~22	—	521.39 (n = 20)	—	[10,22]
3	Chajiasi	30	37.51 (n = 8)	436.19 (n = 13)	42.97 (n = 13)	[23]
4	Yare	25~19	45.57 (n = 9)	429.16 (n = 29)	27.31 (n = 29)	[10,24]
5	Xiongba	25~16	63.24 (n = 15)	479.73 (n = 65)	38.79 (n = 65)	[3,10,16,22]
6	Xuena	19~16	33.21 (n = 4)	298.81 (n = 5)	18.22 (n = 5)	[10]
7	Sailip	18.5~17.6	39.83 (n = 3)	445.52 (n = 12)	26.27 (n = 9)	[6,10,25]
8	Maiga Township	17~16	—	475.79 (n = 12)	—	[26,27]
9	Zabuye	19~15	31.45 (n = 12)	429.18 (n = 34)	29.79 (n = 34)	[10,28]
10	Bugasi	16.2~15.5	—	675.79 (n = 12)	—	[29]
11	Konglong Township	21.3~20.1	—	676.5 (n = 13)	44.85 (n = 12)	[12]
12	Gongmutang	16.5~16.3	—	492.27 (n = 6)	—	[27,28]
13	Cuoqin County	20~15	—	419.42 (n = 14)	24.89 (n = 14)	[29]
14	Xurucuo	11.5	32.77 (n = 4)	649.21 (n = 2)	25.49 (n = 2)	[10]
15	Dangreyongcuo	14.2~13.5	—	624.19 (n = 4)	39.18 (n = 4)	[22]
16	Wenbu	23	—	405.6 (n = 6)	13.4 (n = 6)	[4]
17	Chazi	13.3	41.27 (n = 6)	579.18 (n = 30)	26.87 (n = 30)	[4,10,30]
18	Yiqian	13.5	31.19 (n = 3)	1049.5 (n = 3)	105.54 (n = 3)	[26]
19	Mibale	13.2~12.3	—	494.72 (n = 9)	—	[27]
20	Pabbai zong	18~13	—	363.98 (n = 9)	—	[21]
21	Nanmulin	15.3~14	76.65 (n = 6)	215.56 (n = 4)	20.01 (n = 8)	[31,32]
22	Majiang	21.29~10.1	—	352.59 (n = 6)	—	[1,33]
23	Yangying	11~10.7	33.63 (n = 4)	282.67 (n = 10)	84.93 (n = 10)	[10]

3. Volcanic Rock Types and Dilute Alkali Element Content in the Lhasa Block

3.1. Classification of Volcanic Rocks

We remove the loss on ignition (LOI) of the major element data of volcanic rocks and input the converted data into the Nb/Y-SiO₂ diagram (Figure 2a). The diagram shows that most data were plotted in trachyandesite, trachyte, comendite, and rhyolite dacite areas, and some data were plotted in rhyolite and phonolite areas. In the SiO₂-K₂O diagram (Figure 2b), the potassic-ultrapotassic volcanic rocks samples in the Lhasa block were all plotted in the high K calc-alkaline volcanic rocks series and the shoshonite volcanic rocks series areas.

3.2. Li, Rb, and Cs Contents in Potassic-Ultrapotassic Volcanic Rocks

The abundances of Li, Rb, and Cs in the crust are 20 ppm, 78 ppm, and 2.6 ppm, respectively. The average value of Li content in potassic-ultrapotassic volcanic rocks in the Lhasa block is 46.39 ppm, which is 2.32 times that of the crustal abundance, with 87 sets of data; the average Rb content is 517.23 ppm, which is 6.63 times the crustal abundance, with 324 sets of data; the average content of Cs is 40.43 ppm, which is 15.55 times that of the crustal abundance, with 202 sets of data (Table 1, Figure 4). The above data indicate that not only are dilute alkali elements Li, Rb, and Cs hyperenriched in the potassic-hyperpotassic volcanic rocks of the Lhasa block, but there are also more obvious Li, Rb, and Cs hyperenriched areas that formed in the central and western parts (Li > 2 times, Rb > 5 times, Cs > 7 times). The ages of volcanic rocks are concentrated between 25 and 13 Ma (Table 1, Figures 1 and 4).

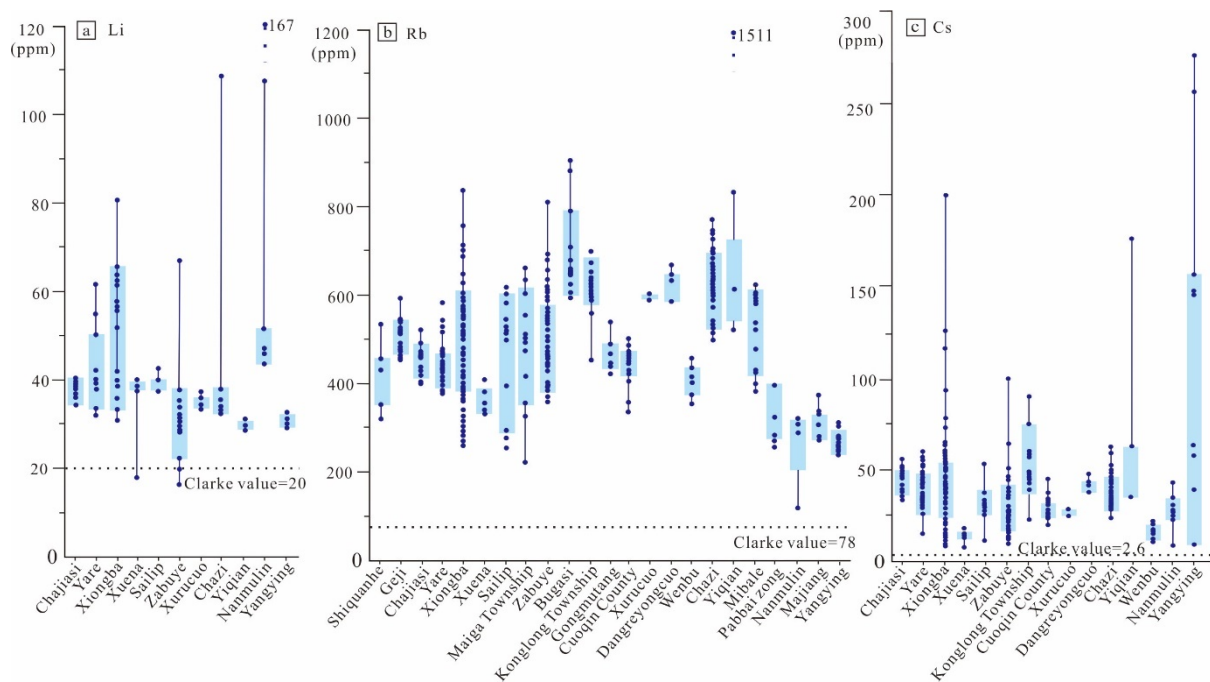


Figure 4. Dilute alkali elements content variation range of potassic-ultrapotassic volcanic rocks in the Lhasa block: (a) Li; (b) Rb; (c) Cs. The wider and light blue ranges represent the distance between the upper and lower quartiles of the sample data.

4. Exploration of the Mechanism of Hyperenrichment of Dilute Alkali Elements

4.1. Characteristics of Major and Trace Elements

In the diagram of the major element analysis, TiO₂ shows a significant negative correlation with SiO₂, possibly reflecting the differentiation of rutile (Figure 5a). The negative correlation between P₂O₅ and SiO₂ may be affected by the differentiation of apatite minerals (Figure 5h). The obvious negative correlation between Zr and SiO₂ (Figure 5j) may

be related to the differentiation of zircon [34]. In addition, Fe^{T} , Eu, CaO, and MgO in the potassic-ultrapotassic volcanic rocks in the Lhasa block exhibited a significant negative correlation with SiO_2 , suggesting that the fractional crystallization of mafic minerals occurred during the magmatic evolution (Figure 5c–e,g). The Dy/Yb and Sr/Y ratios do not show a significant linear correlation with SiO_2 (Figure 5k,l); A/CNK, Na_2O , and Al_2O_3 all show a positive correlation with SiO_2 (Figure 5b,f,i), indicating the clear differentiation of alkaline feldspar.

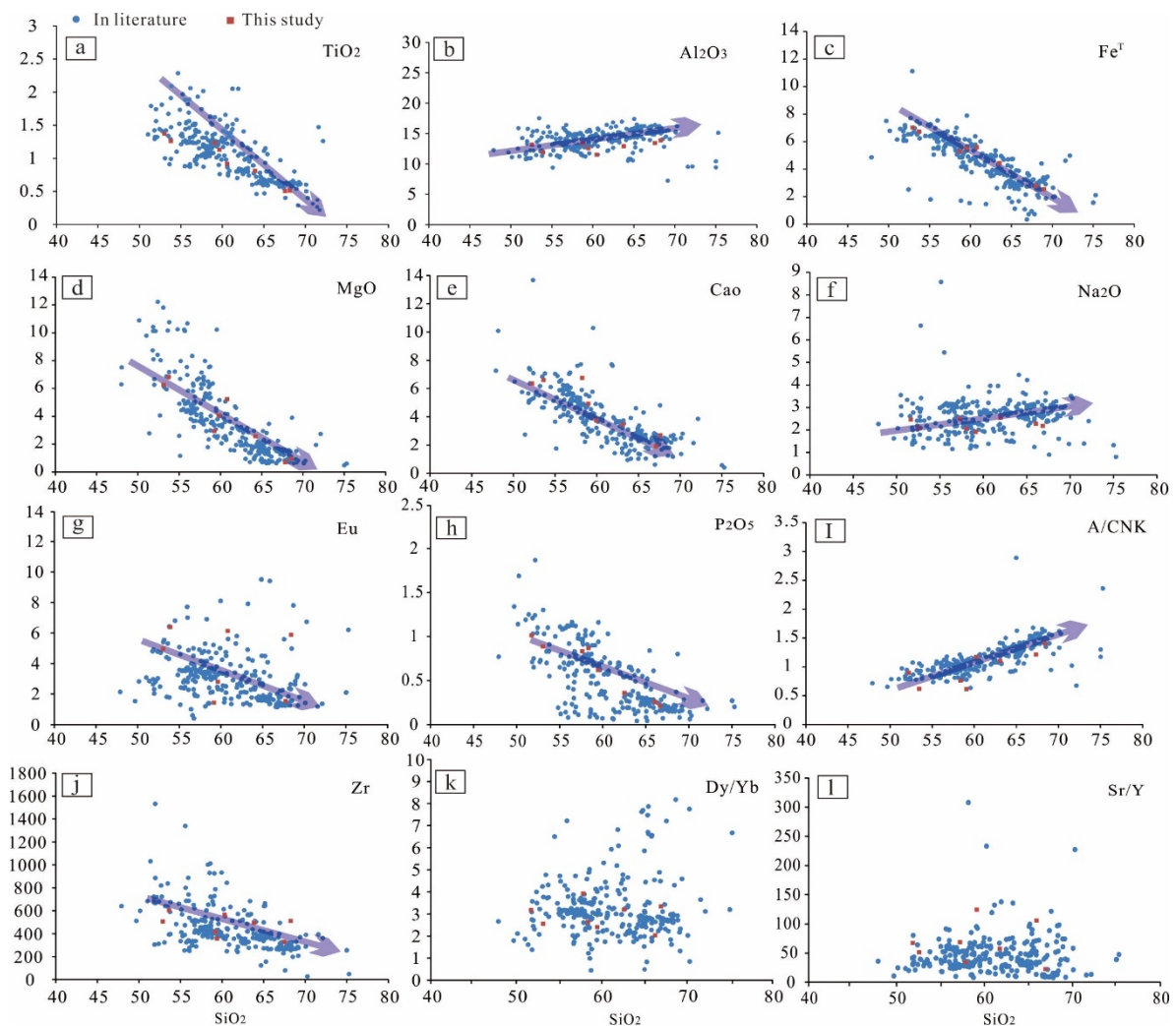


Figure 5. Harker diagram of potassic-ultrapotassic volcanic rocks in the Lhasa block. (a,c–e,g,h,j) TiO_2 , Fe^{T} , Eu, P_2O_5 , CaO, Zr, and MgO have a significant negative correlation with SiO_2 ; (b,f,i) A/CNK, Na_2O , and Al_2O_3 have a positive correlation with SiO_2 ; (k,l) Dy/Yb and Sr/Y ratios do not show a significant linear correlation with SiO_2 . The source of literature data is the same as that in Table 1.

In chondrite-normalized rare earth element (REE) distribution patterns of the potassic-ultrapotassic volcanic rocks in the Lhasa block, LREE (256.9–1489.5 ppm) is relatively enriched, HREE (13.4–67.1 ppm) is relatively depleted, and Eu is weakly depleted (Figure 6a). The weak Eu depletion may be related to the differentiation of plagioclase. The potassic-ultrapotassic volcanic rock samples from the Lhasa block show the strong enrichment of large-ion incompatible elements such as Th and Ce and a strong loss of high-field-strength elements such as Nb, Ta, and Ti in the primitive mantle-normalized trace element spider diagrams (Figure 6b). In addition, it also shows a more obvious tetrad effect with respect to rare earth elements (Figure 6).

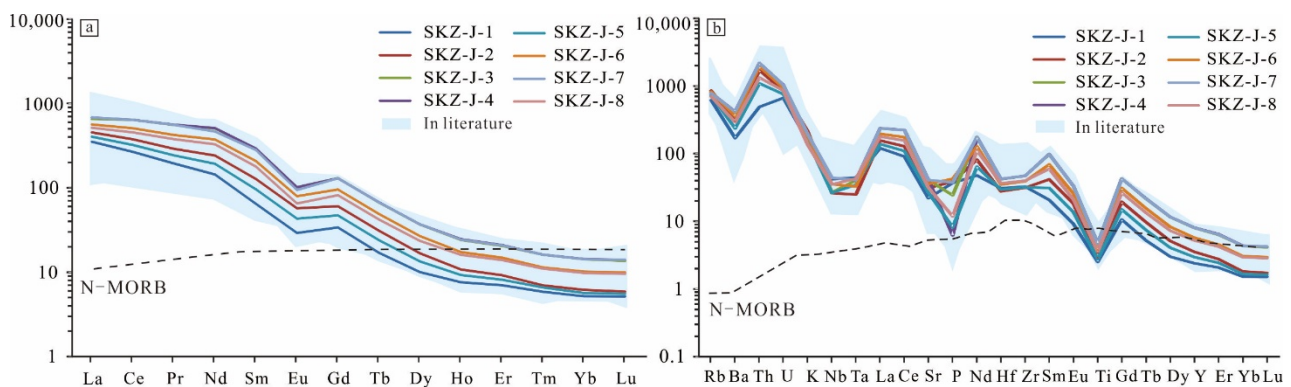


Figure 6. (a) REE pattern of the studied potassic-ultrapotassic volcanic rocks; (b) spider diagram of the studied potassic-ultrapotassic volcanic rocks (chondrites values and N-MORB values sourced from Sun and McDonough [35]). The source of literature data is the same as that in Table 1.

4.2. Ratio Characteristics of Key Elements

Rb does not occur as a separate mineral in nature, most Rb in the crust is hosted in potassium minerals, and the enrichment degree of Rb is generally higher than that of K with the evolution of magma. The K/Rb ratio is an important indicator of differentiation trends in most igneous rocks [36], which can indicate the source of materials and the differentiation history of the upper mantle. The relationship between the K/Rb ratio and K indicates that the ratio decreases with increasing differentiation [8,36,37].

Casting samples of potassic-ultrapotassic volcanic rocks into the K_2O -Rb diagram, it is evident that the Rb content shows a clear upward trend with increasing K_2O content (Figure 7a). In the K-K/Rb diagram, the average K/Rb ratio is 128.06 ($n = 324$), ranging from 33.77 to 235.33 (Figure 7b), and the uniformly low K/Rb ratio may be caused by magmatic differentiation.

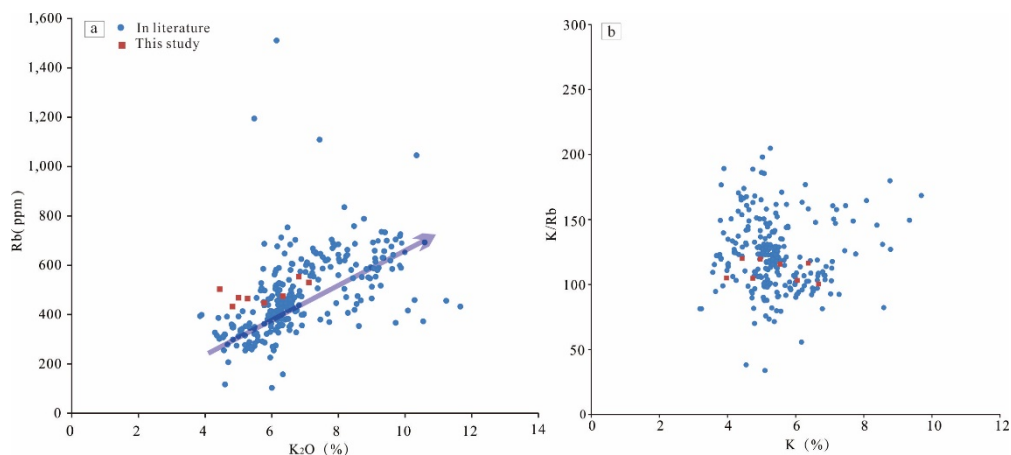


Figure 7. (a) K_2O versus Rb diagram; (b) K versus K/Rb diagram of potassic-ultrapotassic volcanic rocks. The source of literature data is the same as that in Table 1.

The Rb element is concentrated in the residual fluid during the fractional crystallization of magma and will eventually enter potassium minerals; the Sr element was mainly concentrated in the early-formed calcareous plagioclase. Therefore, the Rb/Sr ratio of differentiated igneous rocks increases with the degree of differentiation. The concentrations of Rb and Sr reflect the differentiation degree of residual magma during crystallization. In the diagram of the differentiation degree, Sr concentrations initially decrease very slightly but decrease significantly faster with increasing differentiations; Rb concentrations initially increase very slightly but increase significantly in highly differentiated rocks (Figure 8a).

The Rb/Sr ratio increases very slowly at first and increases sharply with increasing differentiation (Figure 8b).

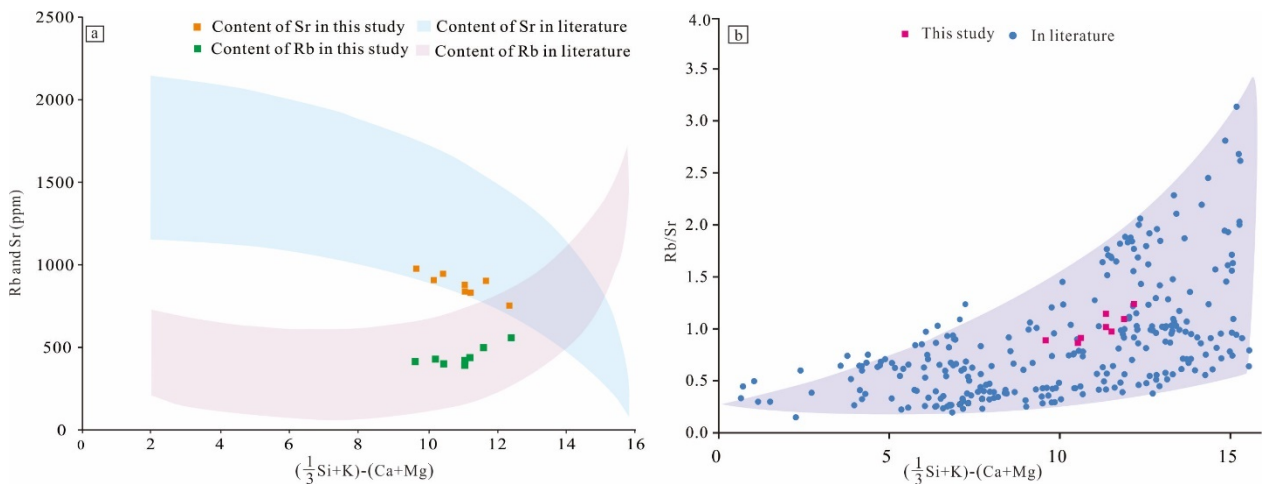


Figure 8. Degree of differentiation of the residual liquid of magma versus Rb and Sr (a) and versus Rb/Sr (b) in potassic-ultrapotassic volcanic rocks. The source of literature data is the same as that in Table 1.

The ratios of geochemically consistent elements such as K/Rb and Nb/Ta do not change in general magmatic systems [38], but these ratios will decrease significantly when properties change significantly due to magmatic differentiation [39]. The parameters related to the differentiation degree of potassic-ultrapotassic volcanic rocks in the Lhasa block are significantly lower than those of chondrites, and they have a higher differentiation index ($DI = 88.4\text{--}95.1$, calculated by CIPW), which may suggest that a higher degree of differentiation occurred (Figure 9).

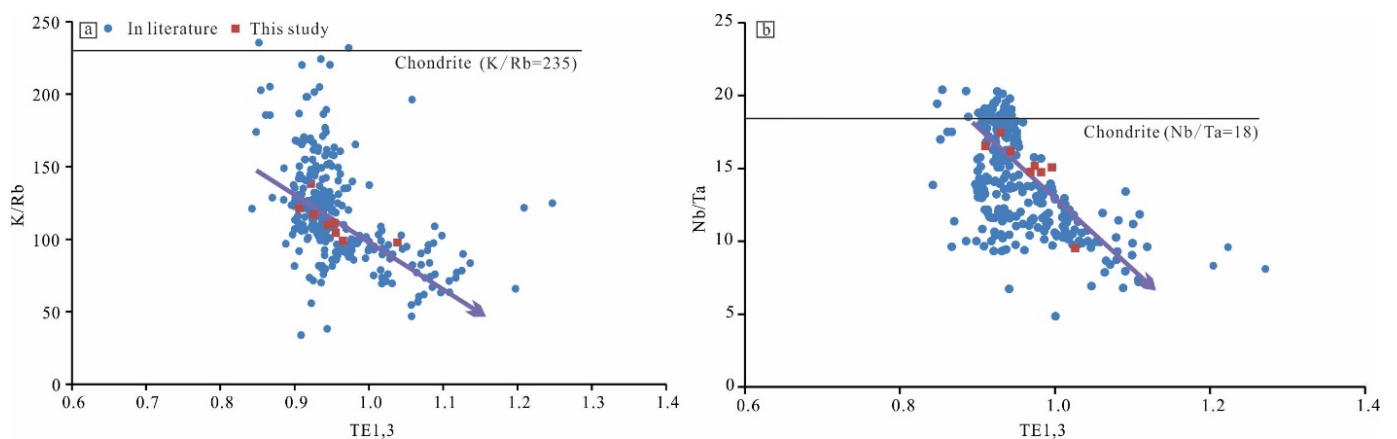


Figure 9. Key element correlation diagrams: (a) represents TE1, 3 versus K/Rb; (b) represents TE1, 3 versus Nb/Ta (chondrite value sourced from Sun and McDonough [35]). The source of literature data is the same as that in Table 1.

4.3. Magmatic Evolution

The quantitative modelling of minerals' fractional crystallization trend was carried out with the help of the Rayleigh fractionation model and distribution coefficient for specific elements between different melt and mineral phases [13] (Figure 10). The potassic-ultrapotassic volcanic rocks of the Lhasa block show a clear trend of separation and crystallization of plagioclase and potassium feldspar in the Sr-Ba diagram (Figure 10a); the Hf/Sm-Zr/Y diagram shows an obvious trend with respect to the separated crystallization

of zircon (Figure 10b); the La- $(La/Yb)_N$ diagram shows a clear trend of separation and the crystallization of monazite, sphene, and apatite (Figure 10c); the Eu-Sr diagram shows a trend with respect to the segregated crystallization of biotite and plagioclase (Figure 10d). In summary, it is speculated that the magma evolution process of volcanic rocks experienced the fractional crystallization of potassium feldspar, plagioclase, biotite, titanite, monazite, apatite, and zircon.

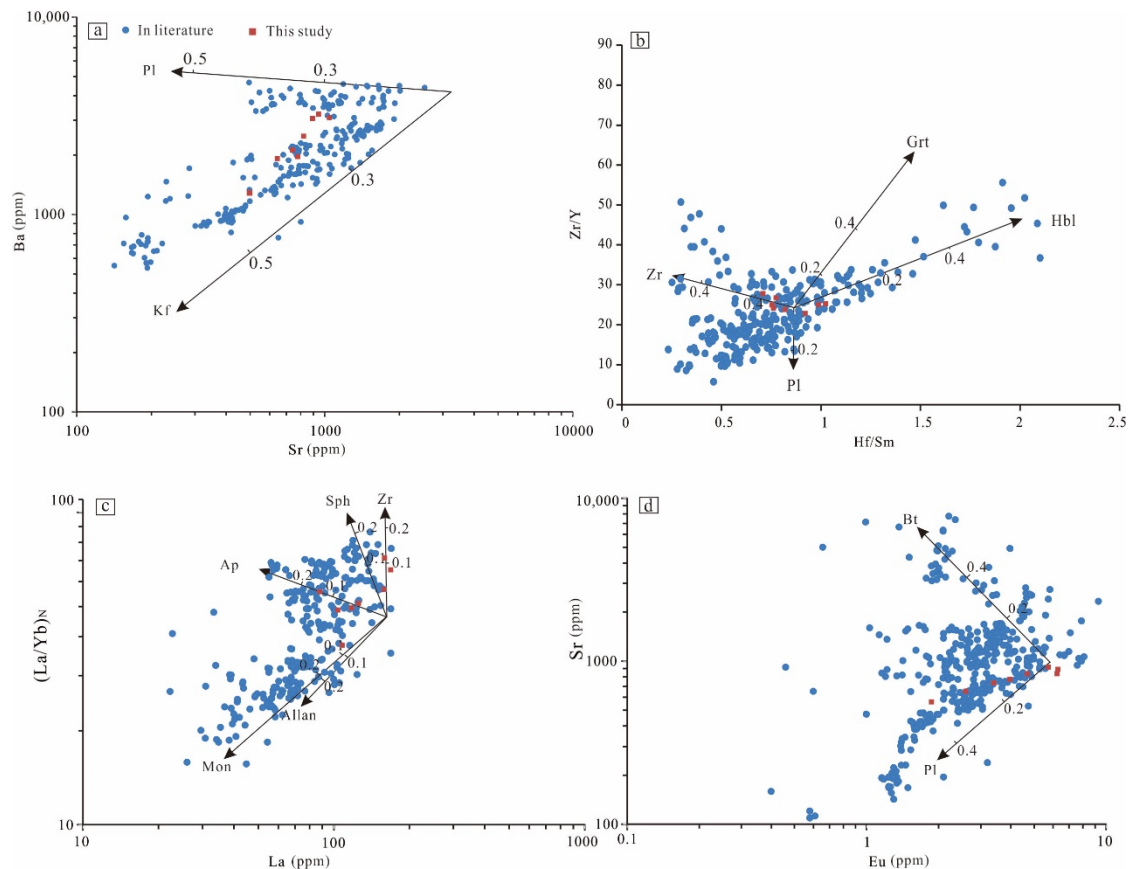


Figure 10. Fractional crystallization discrimination diagram of minerals; (a) represents Sr versus Ba (after Xu et al. [40]); (b) represents Hf/Sm versus Zr/Y (after Xu et al. [40]); (c) represents La versus $(La/Yb)_N$ (after Li et al. [41]); (d) represents Eu versus Sr (after Xiang et al. [42]); crystallized trend of minerals sourced from Wang et al. [43,44]. The source of literature data is the same as that in Table 1. Aln = allanite; Hbl = hornblende; Ap = apatite; Bt=biotite; Grt = garnet; Kf = feldspar; Mnz = monazite ; Pl = plagioclase; Zr = zircon; Sph = sphene.

5. Discussion

5.1. Magmatic Evolution and Fractional Crystallization

Li, Rb, and Cs are strongly incompatible elements, and their enrichment degree will increase with the evolution of magma from basic to acid rocks [45,46]. The SiO_2 content of potassic-ultrapotassic volcanic rocks in the Lhasa block ranges from 47.92% to 75.3%, which is lower than the primitive mantle, with MgO (0.45%–12.5%) and $Mg^\#$ (23.74–51.15), and compatible elements such as Co (2.69 ppm–36.1 ppm) and Ni (3.70 ppm–231 ppm) [10], suggesting that these rocks may be formed by differentiation of magma. There is a significant negative correlation between Eu and SiO_2 (Figure 5g) and significant negative anomalies for both Ba and Eu (Figure 6a,b). Therefore, strong plagioclase separation and crystallization may have occurred during the magmatic evolution process (Figure 10a), which is consistent with the phenomenon of Rb enrichment and high Rb/Sr ratio in residual magma caused by plagioclase differentiation (Figure 8b). The negative correlation between TiO_2 and SiO_2 and the loss of Ti may reflect the differentiation of rutile (Figures 3e, 5a and 6b). The negative

correlation between P_2O_5 and SiO_2 and the loss of P may be due to the differentiation of apatite (Figure 5h, Figure 6b, and Figure 10c).

With the negative correlation between Zr and SiO_2 and the depletion in the trace element's spider diagram (Figures 5j and 6b), the Zr/Hf ratio decreases as Rb/Sr increases and this may be related to the differentiation of zircon (Figure 10b) [34]. On the chondrite-normalized REE distribution diagram, it shows a right-leaning pattern with respect to LREE enrichment, showing a negative Eu anomaly (Figure 6a), which may be related to the interaction between potassium feldspar or plagioclase and solution. In addition, Fe^T , MgO, and CaO all show significant negative correlations with SiO_2 in the potassic-ultrapotassic volcanic rocks of the Lhasa block (Figure 5c–e), suggesting that there is obvious separation and crystallization of mafic minerals in the magmatic evolution process. Garnet partitioning would normally result in Sr/Y and Dy/Yb ratios increasing with SiO_2 [47]; however, Dy/Yb and Sr/Y ratios indicate that garnet partitioning was not evident during magmatic evolution (Figure 5k,l, and Figure 10b). A/CNK, Na_2O , and Al_2O_3 all show a positive correlation with SiO_2 (Figure 5b,f,i), indicating the clear differentiation of alkaline feldspar. The La element shows a tendency to decrease with magmatic evolution (Appendix A), which may be due to the stronger control of LREEs due to monazite and allanite [48] (Figure 10c). Ba tends to occur in K-feldspar, and the crystallization of K-feldspar leads to lower Ba and Ba/Sr ratios in the residual magma; Sr tends to occur in plagioclase, and the fractional crystallization of plagioclase leads to lower Sr and higher Ba/Sr ratios in the residual magma [41]. Hornblende is an important mafic mineral with MREEs (Sm, Eu, Gd), and the relatively flat medium rare earth distribution pattern and roughly equivalent Ho_N and Yb_N values of potassic-ultrapotassic volcanic rocks suggest that there may be hornblende differentiation (Figure 6a). The discrimination of the above differentiation indices is consistent with the observation of plagioclase, hornblende, and biotite as the main phenocryst phases in rock slices.

The tetrad effect of rare earth elements refers to a specific partitioning pattern in the geochemical behavior of REEs in magma after a high degree of magmatic differentiation [49]. There is a low content of REEs in the potassic-ultrapotassic volcanic rocks of the Lhasa block and an obvious rare earth tetrad effect ($TE_{1,3} = 0.86\text{--}1.38$), suggesting that the separation and crystallization of accessory minerals such as monazite, sphene, allanite, and apatite occurred during the magmatic evolution [50] (Figure 9a,b and Figure 10c).

The fractional crystallization of zircons leads to a decrease in Zr and Hf contents and Zr/Hf ratio in magma [51]. The separation of biotite and hornblende enriches the residual magma with Nb and Ta and results in lower Ba/Sr and Nb/Ta ratios [52,53]. The fractional crystallization of rutile and titanite will cause a decrease in Ti, Nb, and Ta contents and an increase in the Nb/Ta ratio in the residual magma [39]. Due to the lower Zr and Nb contents and higher Zr/Hf (~ 34.3) and Nb/Ta (~ 19.9) ratios of the mantle materials [54], the participation of mantle materials will lead to higher Zr/Hf and Nb/Ta ratios and lower Zr and Nb contents in the rock mass, without the trend of a lower Zr/Hf ratio as Zr content decreases (Figure 11a), nor does it explain the trend of increasing Nb and Ta contents as the Nb/Ta ratio decreases (Figure 11b,c). The crustal materials have low Nb and Ta contents, with a Zr/Hf ratio of about 36.7 and an Nb/Ta ratio of about 13.4 [55]. The trend of increasing Nb and Ta contents with decreasing Nb/Ta ratios (Figure 11b,c) indicates that it is not related to the contamination of upper crustal material. Therefore, the differentiation of Zr/Hf and Nb/Ta is not the result of the mantle and crustal materials. Therefore, the fractional crystallization of magma may be the root cause of Zr/Hf and Nb/Ta differentiation.

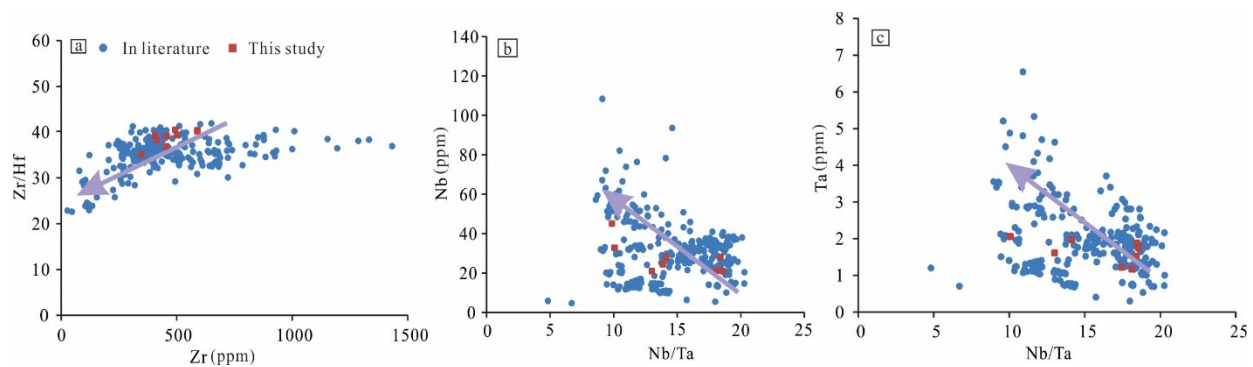


Figure 11. Trace element correlation diagrams for potassic-ultrapotassic volcanic rocks: (a) represents Sr versus Zr/Hf; (b) represents Nb/Ta versus Nb; (c) represents Nb/Ta versus Ta. The source of literature data is the same as that in Table 1.

In summary, there is a high degree of differentiation in the magmatic evolution process of potassic-ultrapotassic volcanic rocks in the Lhasa block. There are mainly some differentiations involving mafic minerals and plagioclase, along with the segregation and crystallization of some monazites and sphenes, while garnets have no obvious separation and crystallization.

5.2. Petrogenesis and Enrichment of Li, Rb, and Cs

The genesis of symbiotic volcanic rock assemblages such as trachyte, trachyandesite, and rhyolitic dacite is generally considered to be caused by basaltic magma differentiation [56]. In the Lhasa block, the slab break-off of the Neo-Tethys oceanic crust during 53–40 Ma triggered substantial mantle-derived basaltic magma underplating [10]. Basaltic magma requires 55% of fractional crystallization to produce trachybasaltic magma and 15% of segregation and crystallization from trachybasaltic magma to produce trachytic magma [57]. Different degrees of crystallization differentiation may be one of the important reasons for the diversity of lithology and geochemical composition of intermediate-acid volcanic rocks.

The geochemical abundance of Rb in the solid crust is closely related to K, and most Rb in nature is dispersed in potassium minerals. Li, Rb, and Cs are strongly incompatible elements and are enriched to a greater degree with the increasing crystallographic differentiation of magma. This increase in enrichment indicates that the rock is more likely to belong to highly differentiated rocks [46]. As the degree of differentiation increases, a large number of potassium-rich minerals appear, providing a carrier for the occurrence of dilute alkali elements. Taking Cs-Ta pegmatites as an example, the enrichment of Rb is 4–10 times and the enrichment of Cs is 16–25 times in the highly differentiated spodumene and lepidolite subclasses. However, in the subclasses with a low degree of differentiation, Rb is only 1-fold enriched and Cs is only 3–5-fold enriched [14]. Li is not enriched in the same type of potassic-ultrapotassic volcanic rocks in the Qiangtang and Hoh Xil blocks formed by post-collision, Rb is only 2 times enriched, and Cs is 2–5 times enriched [5,58–60]. In this area, Li is 2 times enriched, Rb is 6.63 times enriched, and Cs is 15.55 times enriched. Therefore, it is considered that there is a higher degree of differentiation in the potassic-ultrapotassic volcanic rocks in this area.

The age of potassic-ultrapotassic rocks overlaps with the development time of extensional structures in the Lhasa block, indicating that they are genetically related [9]. The same type of magmatism occurred in the same period of time during 25–13 Ma, indicating that these rocks have the same or similar genetic mechanisms, tectonic environments, and magma source material compositions [4]. Regarding the genesis of volcanic rocks, combined with the lithospheric mantle-convection thinning model and the subduction slab break-off model, lithospheric mantle thinning may occur due to upwelling in the asthenosphere, and thermal disturbance caused by slab breakoff [21]. When the lithospheric-thinning

continent began to crack, under the action of stress release, the decompression melting of the lithospheric mantle produced basaltic magma along the tectonic weak zone and upward emplacement and experienced a high degree of separation and crystallization; it finally formed a set of Li-, Rb- and Cs-enriched trachyte-trachyandesite-rhyolite dacite assemblage in the region.

5.3. Comparison between Potassic-Ultrapotassic Volcanic Rocks and Highly Fractionated Granites

The separation of minerals from magma is the key to the change in or differentiation of magma composition [61]. The crystal porridge model holds that granite and rhyolite exhibit complementary liquid-solid relationships of the same space and the same source [62]. According to this theory, since granite can undergo a high degree of crystallization differentiation, the differentiated magma can also erupt to form rhyolite. Highly fractionated granites have the following characteristics: (1) The contents of trace elements such as Ni, Cr, Co, Sr, Ba, and Zr in granitic magma decreased significantly during crystallization differentiation, and the contents of Li, Rb, and Cs increased significantly [46]. (2) The ratios of K/Rb, Zr/Hf, and Nb/Ta decrease significantly when magmatic differentiation occurs [38,39]. (3) The Zr/Hf and Nb/Ta ratios of the entire rock can be used as indicators to determine the degree of crystallization differentiation of granitic magma ($Zr/Hf < 38$ and $Nb/Ta < 17$) [13]. (4) The content of rare earth elements in highly fractionated granites tends to be low, the ratio of light and heavy rare earth elements tends to be small and the negative anomaly of Eu increases, indicating the separation of zircon, monazite, allanite, and feldspar minerals rich in rare earth elements. In addition, they mostly show the tetrad effect of rare earth elements [13].

The strong coherence between K and Rb makes it difficult to use the K/Rb ratio to track the moderate differentiation process. The Ba/Rb ratio is more sensitive than the K/Rb ratio in tracing K-feldspar differentiation [63]. Sr is evenly distributed in the normal granite group, and the content of Ba increases in association with the decreasing content of Rb. The highly fractionated granites exhibited K/Rb ratios in the range from 156 to 207 [37], and potassic-ultrapotassic volcanic rocks in the Lhasa block are 33.77–235.33, with an average of 128.4 and a lower K/Rb ratio. The content of Ba of highly fractionated granites is obviously depleted, but the content of Rb is enriched. Sr in alkaline feldspar easily decreases with differentiation because it replaces Ca in plagioclase and K in K-feldspar, while Ba only replaces K in K-feldspar [64]. In the Rb-Ba-Sr ternary discriminant diagram of highly fractionated granites, the content of Rb in volcanic rock samples shows a significant increasing trend, and it gradually approaches the mapping area of highly differentiated granites (Figure 12a), showing a high degree of differentiation. Casting the potassic-ultrapotassic volcanic rocks' data into the Nb/Ta-Zr/Hf diagram, the distribution range of the Lhasa block's potassic-ultrapotassic volcanic rock data with a higher degree of differentiation is considered to be $Zr/Hf < 40$ and $Nb/Ta < 20$ compared to the distribution range of highly fractionated granites ($Zr/Hf < 38$ and $Nb/Ta < 17$) [13] (Figure 12b).

On the whole, trace elements such as Cr, Ni, Co, Sr, Ba, and Zr were significantly reduced during the crystallization and differentiation of potassic-ultrapotassic volcanic rocks in the Lhasa block, and the ratios of K/Rb, Zr/Hf, and Nb/Ta were significantly reduced. Volcanic rocks were enriched in large-ion incompatible elements and depleted in high-field-strength elements, with obvious rare earth element tetrad effects, a lower K/Rb ratio, and a higher Rb/Sr ratio. The magmatic evolution segregated the crystallization of potassium feldspar, plagioclase, biotite, apatite, rutile, zircon, and other minerals, with a high degree of differentiation.

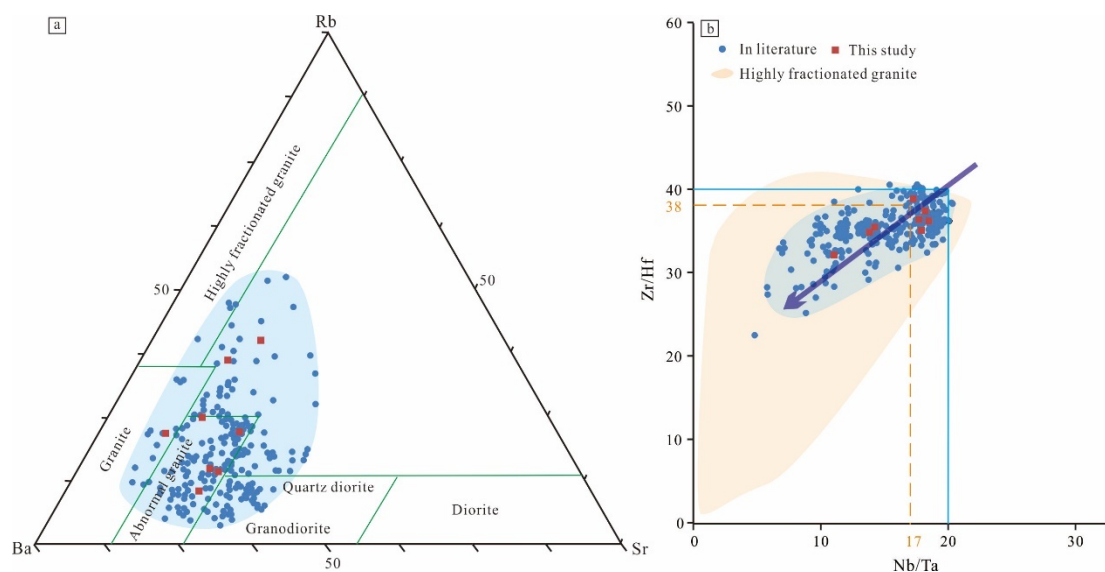


Figure 12. (a) High differentiation discriminant diagram of granites; (b) diagram of Nb/Ta versus Zr/Hf. Highly fractionated granites from Wu [13]. The source of literature data is the same as that in Table 1.

6. Conclusion

1. In the potassic-ultrapotassic volcanic rock samples of the Lhasa block, the average contents of Li, Rb, and Cs were 2.32 times, 6.63 times, and 15.55 times that of the crustal Clark values, respectively, with the extraordinary enrichment of Li, Rb, and Cs. The supernormal enrichment area is mainly distributed in the central and western areas of the Lhasa block, where the age range of the volcanic rocks is between 25 and 13 Ma.
2. The potassic-ultrapotassic volcanic rocks in the Lhasa block are enriched with large-ion incompatible elements and depleted in terms of high-field strength elements, and they exhibit the obvious tetrad effects of rare earth elements. Combined with the indices of element differentiation, this paper proposes that magmatic evolution underwent the segregated crystallization of potassium feldspar, plagioclase, biotite, hornblende, apatite, rutile, zircon, and other minerals.
3. Combining geochemical characteristics and magmatic evolution trends, this paper suggests that a high degree of differentiation exists during magmatic evolution in the potassic-ultrapotassic volcanic rocks of the Lhasa block. The characteristic ratios of elements characterized by high differentiation are $Zr/Hf < 40$ and $Nb/Ta < 20$ compared with other regions.

Author Contributions: Conceptualization, D.C., Y.Z. and M.Z.; methodology, D.C. and Y.Z.; software, D.C., E.X. and M.L.; validation, D.C., E.X. and C.Y.; formal analysis, D.C. and X.Z.; investigation, D.C., Y.Z. and C.Y.; resources, D.C., M.Z. and X.Z.; data curation, D.C., writing—original draft preparation, D.C. and Y.Z.; writing—review and editing, D.C., M.Z., C.Y., Y.Z. and Z.Z.; visualization, D.C. and C.Y.; supervision, M.Z.; project administration, M.Z.; funding acquisition, M.Z. All authors have read and agreed to the published version of the manuscript.

Funding: This work was supported by the National Natural Science Foundation of China (No: 91962219), and the Second Tibetan Plateau Scientific Expedition (STEP) program (award 2022QZKK0201).

Data Availability Statement: Not applicable.

Acknowledgments: We thank the anonymous reviewers whose comments have improved the quality of the manuscript.

Conflicts of Interest: The authors declare no conflict of interest.

Appendix A

Table A1. Major (wt.%) and trace element (ppm) concentrations of the Sekazhi in the Xiongba Basin.

Sample Number	SKZ-J-1	SKZ-J-2	SKZ-J-3	SKZ-J-4	SKZ-J-5	SKZ-J-6	SKZ-J-7	SKZ-J-8
Rock Type	trachyandesite			trachyte			rhyolite dacite	
SiO ₂	59.20	53.30	53.90	64.01	59.40	60.62	68.10	67.40
TiO ₂	1.36	1.42	0.99	0.72	1.20	0.86	0.62	0.62
Al ₂ O ₃	14.00	13.60	12.20	13.90	13.20	12.88	15.30	14.80
Fe ₂ O ₃	5.43	6.96	6.23	4.67	5.46	5.51	2.91	3.08
MnO	0.05	0.10	0.11	0.09	0.07	0.10	0.02	0.05
MgO	3.61	6.08	7.17	2.96	4.38	5.06	0.91	1.27
CaO	6.44	6.16	7.06	3.91	4.25	3.93	2.50	2.01
Na ₂ O	1.27	2.41	2.00	3.44	2.30	2.62	2.95	2.35
K ₂ O	5.00	5.98	6.31	4.40	6.90	6.23	4.85	5.06
P ₂ O ₅	0.90	1.03	0.91	0.30	0.94	0.60	0.16	0.21
LOI	1.58	1.45	1.88	0.11	1.41	1.37	1.02	2.56
Total	98.70	98.40	98.60	98.57	99.70	99.78	99.40	99.30
Li	80.43	74.03	78.03	79.36	70.29	77.76	78.30	75.36
Be	11.88	7.90	8.86	10.37	6.94	8.86	8.86	9.41
Sc	8.92	13.89	17.68	13.30	10.11	17.67	17.68	9.52
Cr	103.90	249.74	341.40	217.41	147.62	351.86	330.93	125.76
Nb	20.69	28.01	34.95	27.88	21.21	34.82	35.08	20.95
Rb	402.83	531.15	511.11	457.45	552.14	510.16	512.06	477.48
Zr	414.03	493.82	590.10	502.26	397.92	589.71	590.49	405.97
Hf	10.84	12.20	14.66	12.77	9.77	14.62	14.70	10.31
Ni	45.34	111.57	153.82	97.02	64.19	158.95	148.70	54.76
Ta	2.05	1.52	1.88	1.97	1.17	1.87	1.88	1.61
Th	43.40	163.56	183.11	113.62	144.74	182.38	183.84	94.07
U	14.35	19.98	21.99	18.24	18.11	21.86	22.13	16.23
Ba	1277.57	2617.12	3027.83	2163.49	2227.98	3006.26	3049.41	1752.78
Sr	533.28	856.60	973.58	756.23	745.21	967.99	979.17	639.25
V	66.53	84.78	101.59	83.63	67.11	102.44	100.73	66.82
Cs	38.21	46.71	49.15	45.23	37.61	40.21	39.13	45.47
Ga	27.43	26.50	27.77	27.62	25.28	27.73	27.82	26.35
Ti	4039.66	6079.31	7383.33	5699.77	4751.83	7406.79	7359.88	4395.75
La	89.76	144.03	172.80	131.61	115.91	172.15	103.45	102.83
Ce	175.76	334.29	421.78	299.06	247.38	421.20	422.36	211.57
Pr	19.88	43.14	56.99	38.59	29.60	56.69	57.29	24.74
Nd	72.24	187.85	255.70	164.59	121.24	254.46	256.94	96.74
Sm	10.60	34.14	47.74	29.34	20.87	47.40	48.08	15.74
Eu	1.81	4.94	6.32	4.06	3.55	6.32	6.31	2.68
Gd	7.46	21.05	28.68	18.03	13.35	28.75	28.60	10.41
Tb	0.68	1.96	2.69	1.69	1.24	2.68	2.70	0.96
Dy	2.72	7.28	10.04	6.40	4.55	10.00	10.07	3.64
Ho	0.46	1.05	1.47	0.97	0.65	1.46	1.49	0.56
Er	1.24	2.64	3.68	2.47	1.63	3.64	3.71	1.44
Tm	0.16	0.31	0.44	0.30	0.19	0.44	0.44	0.18
Yb	0.94	1.85	2.60	1.78	1.12	2.59	2.61	1.03
Lu	0.14	0.27	0.38	0.26	0.16	0.37	0.38	0.15
Y	13.49	31.38	43.48	28.68	19.67	43.10	43.86	16.58

References

1. Coulon, C.; Maluski, H.; Bollinger, C.; Wang, S. Mesozoic and cenozoic volcanic rocks from central and southern Tibet: ³⁹Ar-⁴⁰Ar dating, petrological characteristics and geodynamical significance. *Earth Planet. Sci. Lett.* **1986**, *79*, 281–302. [[CrossRef](#)]
2. Harrison, T.M.; Lovera, O.M.; Grove, M. New insights into the origin of two contrasting Himalayan granite belts. *Geology* **1997**, *25*, 899–902. [[CrossRef](#)]

3. Miller, C.; Schuster, R.; Kltzli, U.; Frank, W.; Purtscheller, F. Post-collisional potassic and ultrapotassic magmatism in SW Tibet: Geochemical and Sr-Nd-Pb-O isotopic constraints for mantle source characteristics and petrogenesis. *J. Petrol.* **1999**, *40*, 1399–1424. [[CrossRef](#)]
4. Ding, L.; Kapp, P.; Zhang, D.; Deng, W.M. Cenozoic volcanism in Tibet: Evidence for a transition from oceanic to continental subduction. *J. Petrol.* **2003**, *40*, 1833–1865. [[CrossRef](#)]
5. Guo, Z.F.; Wilson, M.; Liu, J.Q.; Mao, Q. Post-collisional, potassic and ultrapotassic magmatism of the northern Tibetan Plateau: Constraints on characteristics of the mantle source, geodynamic setting and uplift mechanisms. *J. Petrol.* **2006**, *47*, 1177–1220. [[CrossRef](#)]
6. Sun, C.G.; Zhao, Z.D.; Mo, X.X.; Mo, X.X.; Zhu, D.C.; Dong, G.C.; Zhou, S.; Chen, H.H.; Xie, L.W.; Yang, Y.H.; et al. Enriched mantle source and petrogenesis of Sailipu ultrapotassic rocks in southwestern Tibetan Plateau: Constraints from zircon U-Pb geochronology and Hf isotopic compositions. *Acta Petrol. Sin.* **2008**, *24*, 249–264. (In Chinese)
7. Mo, X.X. *Cenozoic Collisional-Post-Collisional Igneous Rocks of the Qinghai-Tibet Plateau*; Geological Press: Beijing, China, 2009; pp. 1–342. (In Chinese)
8. Murray, M.M.; Rogers, J.J. Distribution of rubidium and strontium in the potassium feldspars of two granite batholiths. *Geochem. J.* **1973**, *6*, 117–130. [[CrossRef](#)]
9. Zhao, Z.; Chi, X.G.; Liu, J.F.; Li, G.R.; Zhao, Y.D. Geochemical feature and its tectonic significance of Gemucuo Oligocene potassic volcanic rocks in the Qiangtang area, Tibet, China. *Geol. Bull. China* **2009**, *28*, 463–473. (In Chinese)
10. Liu, D. Geochemistry and Petrogenesis of the Postcollisional Potassic-Ultrapotassic Rocks in Tibetan Plateau. Ph.D. Thesis, China University of Geosciences (Beijing), Beijing, China, 2017. (In Chinese).
11. Turner, S.; Arnaud, N.; Liu, J.; Rogers, N.; Hawkesworth, C.; Harris, N.; Kelley, S.; Calsteren, P.; Deng, W. Post-collision, shoshonitic volcanism on the Tibetan Plateau: Implications for convective thinning of the lithosphere and the source of ocean island basalts. *J. Petrol.* **1996**, *37*, 45–71. [[CrossRef](#)]
12. Chen, J.L.; Xu, J.F.; Wang, B.D.; Kang, Z.Q.; Li, J. Origin of Cenozoic alkaline potassic volcanic rocks at Konglong Xiang, Lhasa terrane, Tibetan Plateau: Products of partial melting of a mafic lower crustal source? *Chem. Geol.* **2010**, *273*, 286–299. [[CrossRef](#)]
13. Wu, F.Y.; Lu, X.Y.; Ji, W.Q.; Wang, J.M.; Yang, L. Identification and study of highly differentiated granites. *Sci. China Press* **2017**, *47*, 745–765. (In Chinese)
14. Gao, L.E.; Zeng, L.S.; Yan, L.L.; Zhao, L.H.; Li, G.X.; Di, Y.L.; Wang, Y.Y.; Wang, H.T. Changes in the melt structure and enrichment of rare metals W-Sn-Nb-Ta in granitic magma: An example from the Xiaru Early Paleozoic granites. *Acta Petrol. Sin.* **2022**, *38*, 3281–3301. (In Chinese) [[CrossRef](#)]
15. Yang, H.; Lai, S.C.; Qin, J.F. Geochemical characteristics of alkali trachytes in Ziyang-Langao area, north daba mountains and petrogenetic relation with the diabbases. *Geotecton. Metallog.* **2021**, *45*, 413–424. (In Chinese) [[CrossRef](#)]
16. Zheng, M.P.; Chen, W.X.; Qi, W. New findings and perspective analysis of prospecting for volcanic sedimentary boron deposits in the Tibetan Plateau. *Acta Geosci. Sin.* **2016**, *37*, 407–418. (In Chinese)
17. Winchester, J.A.; Floyd, P.A. Geochemical discrimination of different magma series and their differentiation products using immobile elements. *Chem. Geol.* **1977**, *20*, 325–343. [[CrossRef](#)]
18. Peccerillo, R.; Taylor, S.R. Geochemistry of eocene calc-alkaline volcanic rocks from the Kastamonu area northern Turkey. *Contrib Mineral. Petrol.* **1976**, *58*, 63–81. [[CrossRef](#)]
19. Zhang, R. Petrogenesis of the Cenozoic Alkaline Potassic Ultrapotassic Volcanic Rocks from Qiangtang, Northern Tibet. Ph.D. Thesis, Jin Lin University, Changchun, China, 2018. (In Chinese).
20. Dong, Y.H.; Wang, Q.; Xu, J.F.; Zi, F. Dongyue lake adakitic volcanic rocks with high Mg in north Qiangtang block: Petrogenesis and its tectonic implication. *Acta Petrol. Sin.* **2008**, *24*, 291–302. (In Chinese)
21. Williams, H.M.; Turner, S.P.; Pearce, J.A.; Kelley, S.P.; Harris, N.B.W. Nature of the source regions for post-collisional, potassic magmatism in southern and northern Tibet from geochemical variations and inverse trace element modelling. *J. Petrol.* **2004**, *45*, 555–607. [[CrossRef](#)]
22. Zhang, Y.L. Geological Characteristics of Cenozoic Volcanic Rocks and Its Geodynamic Implication in Shiquanhe-Geze Area on Qinghai-Tibet Plateau. Ph.D. Thesis, China University of Geoscience (Beijing), Beijing, China, 2018. (In Chinese).
23. Hu, W.J.; Tian, S.H.; Yang, Z.S.; Zhang, Z.Q. Petrogenesis of Miocene Chajiasi potassic rocks in western Lhasa block Tibetan Plateau: Constraints from litho geochemistry, geochronology and Sr-Nd isotopes. *Miner. Depos.* **2012**, *31*, 813–830. (In Chinese)
24. Nomade, S.; Renne, P.R.; Mo, X.X.; Zhao, Z.D.; Zhou, S. Miocene volcanism in the Lhasa block, Tibet: Spatial trends and geodynamic implications. *Earth Planet. Sci. Lett.* **2004**, *221*, 227–243. [[CrossRef](#)]
25. Wang, B.D.; XU, J.F.; Zhang, X.G.; Chen, J.L.; Kang, Z.Q.; Dong, Y.H. Petrogenesis of Miocene volcanic rocks in the Sailipu area Western Tibetan Plateau: Geochemical and Sr-Nd isotopic constraints. *Acta Petrol. Sin.* **2008**, *24*, 265–278. (In Chinese)
26. Ding, L.; Yue, Y.H.; Cai, F.L.; Xu, X.X.; Zhang, Q.H.; Lai, Q.Z. $^{40}\text{Ar}/^{39}\text{Ar}$ Geochronology, Geochemical and Sr-Nd-O isotopic characteristics of the high-Mg ultrapotassic rocks in Lhasa block of Tibet: Implications in the onset time and depth of NS-striking Rift System. *Acta Geol. Sin.* **2006**, *8*, 1252–1352. (In Chinese)
27. Liu, Y.F.; Xu, L.F.; Zhang, Z.F.; Chen, L.L.; Huang, F.; Zhu, H.L.; Liu, F. Ca-Mg isotopic compositions of ultra Potassic volcanic rocks in the Lhasa terrane, Southern Tibet and their geological implications. *Acta Geol. Sin.* **2018**, *92*, 545–559. (In Chinese)
28. Jiang, Y.S.; Zhou, Y.Y.; Wang, M.G.; Xie, Y.X.; Li, J.B.; Peng, B. Characteristics and geological significance of Quaternary volcanic rocks in the central segment of the Gangdise area. *Geol. Bull. China* **2003**, *22*, 16–21. (In Chinese)

29. Chen, J.L.; Xu, J.F.; Kang, Z.Q.; Wang, B.D. Origin of the Miocene Bugasi Group volcanic rocks in the Cuoqin County, Western Tibetan Plateau. *Acta Petrol. Sin.* **2006**, *22*, 585–594. (In Chinese)
30. Chen, J.L.; Xu, J.F.; Kang, Z.Q.; Wang, B.D. Geochemistry and origin of Miocene volcanic rocks in Cazé area south-western Qinghai-Xizang plateau. *Geochimica* **2007**, *36*, 457–466. (In Chinese)
31. Xu, L.K. Chronology, Geochemistry and Rock Genesis of Potassium-Ultrapotassium Volcanic Rocks in the Temple Group of the Middle Section of Lhasa Block. Master's Thesis, Chengdu University of Technology, Chengdu, China, 2019. (In Chinese).
32. Zhao, Z.D.; Mo, X.X.; Zhang, S.Q.; Guo, T.Y.; Zhou, S.; Dong, G.C.; Wang, Y. Post-collisional magmatism in the Wuyu Basin, central Tibet Evidence for subduction and recirculation of a Tethys oceanic crust. *Sci. China (Ser. D)* **2001**, *31*, 20–27. (In Chinese)
33. Wang, B.D.; Chen, L.K.; Xu, J.F.; Liu, H.F.; Chen, J.L.; Kang, Z.Q. Identification and petrogenesis of potassic volcanic rocks with “ultrapotassic” characteristics from Maqiang area in Lhasa block. *Acta Petrol. Sin.* **2011**, *27*, 1662–1674. (In Chinese)
34. King, P.L.; White, A.R.; Chappell, B.W.; Allen, C.M. Characterization and origin of aluminous A-type granites from the Lachlan Fold Belt, southeastern Australia. *J. Petrol.* **1997**, *38*, 371–391. [[CrossRef](#)]
35. Sun, S.S.; McDonough, W.F. Chemical and isotopic systematics of oceanic basalts: Implications for mantle composition and processes. In *Magmatism in the Ocean Basins*; Saunders, A.D., Norry, M.J., Eds.; Geological Society, London, Special Publication: London, UK, 1989; Volume 42, pp. 313–345. [[CrossRef](#)]
36. Taubeneck, W.H. An appraisal of some potassium-rubidium ratios in igneous rocks. *J. Geophys. Res.* **1965**, *70*, 475–479. [[CrossRef](#)]
37. Ahrens, L.H.; Pinson, W.H.; Kearns, M.M. Association of rubidium and potassium and their abundance in common igneous rocks and meteorites. *Geochim. Cosmochim. Acta* **1952**, *2*, 229–242. [[CrossRef](#)]
38. Green, T.H. Significance of Nb/Ta as an indicator of geochemical processes in the crust-mantle system. *Chem. Geol.* **1995**, *120*, 347–359. [[CrossRef](#)]
39. Linnen, R.L.; Keppler, H. Melt composition control of Zr/Hf fractionation in magmatic processes. *Geochim. Cosmochim. Acta* **2002**, *66*, 3293–3301. [[CrossRef](#)]
40. Xu, B.; Jiang, S.Y.; Wang, R.; Ma, L.; Zhao, K.D.; Yan, X. Late Cretaceous granites from the giant Dulong Sn-poly-metallic ore district in Yunnan Province, South China: Geochronology, geochemistry, mineral chemistry and Nd-Hf isotopic compositions. *Lithos* **2015**, *219*, 54–72. [[CrossRef](#)]
41. Li, Y.L.; Zhang, H.F.; Guo, J.H.; Li, C.F. Petrogenesis of the Huili Paleo proterozoic leucogranite in the Jiaobei Terrane of the North China Craton: A highly fractionated albite granite forced by K-feldspar fractionation. *Chem. Geol.* **2017**, *450*, 165–182. [[CrossRef](#)]
42. Xiang, Y.; Yang, J.H.; Chen, J.Y.; Zhang, Y. Petrogenesis of Lingshan highly fractionated granites in the Southeast China: Implication for Nb-Ta mineralization. *Ore Geol. Rev.* **2017**, *89*, 495–525. [[CrossRef](#)]
43. Rollinson, H.R. *Using Geochemical Data: Evaluation, Presentation, Interpretation*; Longman: Harlow, UK, 1993; pp. 1–325. [[CrossRef](#)]
44. Yurimoto, H.; Duke, E.F.; Papike, J.J.; Shearer, C.K. Are discontinuous chondrite-normalized REE patterns in pegmatitic granite systems the results of monazite fractionation? *Geochim. Cosmochim. Acta* **1990**, *54*, 2141–2145. [[CrossRef](#)]
45. Barros, R.; Kaeter, D.; Menuge, J.F.; Skoda, R. Controls on chemical evolution and rare element enrichment in crystallising albite-spodumene pegmatite and wallrocks: Constraints from mineral chemistry. *Lithos* **2020**, *19*, 1–58. [[CrossRef](#)]
46. Lee, C.T.; Morton, D.M. High silica granites: Terminal porosity and crystal settling in shallow magma chambers. *Earth Planet. Sci. Lett.* **2015**, *409*, 23–31. [[CrossRef](#)]
47. Castillo, P.R.; Janney, P.E.; Solidum, R.U. Petrology and geochemistry of Camiguin island, southern Philippines: Insights to the source of adakites and other lavas in a complex arc setting. *Contrib. Mineral. Petrol.* **1999**, *134*, 33–51. [[CrossRef](#)]
48. Bea, F. Residence of REE, Y, Th and U in granites and crustal protoliths: Implications for the chemistry of crustal melts. *J. Petrol.* **1996**, *37*, 521–552. [[CrossRef](#)]
49. Jahn, B.M.; Wu, F.Y.; Capdevila, R.; Martineau, F.; Zhao, Z.H.; Wang, Y.X. Highly evolved juvenile granites with tetrad REE patterns: The Woduhe and Baerzhe granites from the Great Xing'an Mountains in NE China. *Lithos* **2001**, *59*, 171–198. [[CrossRef](#)]
50. Irber, W. The lanthanide tetrad effect and its correlation with K/Rb, Eu/Eu*, Sr/Eu, Y/Ho, and Zr/Hf of evolving peraluminous granite suites. *Geochim. Cosmochim. Acta* **1999**, *63*, 489–508. [[CrossRef](#)]
51. Watson, E.B.; Harrison, T.M. Zircon saturation revisited: Temperature and composition effects in a variety of crustal magma. *Earth Planet. Sci. Lett.* **1983**, *64*, 295–304. [[CrossRef](#)]
52. Tiepolo, M.; Vannucci, R.; Oberti, R.; Foley, S.; Zanetti, A. Nb and Ta incorporation and fractionation in titanite and kaersutite: Crystal-chemical constraints and implications for natural systems. *Earth Planet. Sci. Lett.* **2000**, *176*, 185–201. [[CrossRef](#)]
53. Stepanov, A.S.; Mavrogenes, J.A.; Meffre, S.; Davidson, P. The key role of mica during igneous concentration of tantalum. *Contrib. Mineral. Petrol.* **2014**, *167*, 1009. [[CrossRef](#)]
54. Munker, C.; Pfander, J.A.; Weyer, S.; Buchl, A.; Kieine, T.; Klaus, M. Evolution of planetary cores and the earth-moon system from Nb/Ta systematics. *Science* **2003**, *301*, 84–87. [[CrossRef](#)] [[PubMed](#)]
55. Rudnick, R.L.; Gao, S. Composition of the continental crust. *Treatise Geochem.* **2004**, *4*, 1–51. [[CrossRef](#)]
56. Dmitrienko, L.V.; Wang, P.C.; Li, S.Z.; Cao, X.Z.; Somerville, I.; Zhou, Z.Z.; Hu, M.Y.; Suo, Y.H.; Guo, L.L.; Wang, Y.M.; et al. Meso-Cenozoic Evolution of Earth Surface System under the East Asian Tectonic Superconvergence. *Acta Geol. Sin.-Engl. Ed.* **2018**, *92*, 814–849. [[CrossRef](#)]
57. Clague, D.A. The oceanic basalt-trachyte association: An explanation of the Daly gap. *J. Geol.* **1978**, *86*, 5. [[CrossRef](#)]
58. Lai, S.C.; Liu, C.Y.; Song, Y.O. The genesis of the Neotertiary high-potassium calc-alkaline volcanic system of North Qiangtang and its continental dynamics significance. *Sci. China (Ser. D)* **2001**, *31*, 34–42. (In Chinese)

59. Jiang, D.H.; Liu, J.Q.; Ding, L. Geochemistry and petrogenesis of Cenozoic potassic volcanic rocks in the Hoh Xil area northern Tibet Plateau. *Acta Petrol. Sin.* **2008**, *24*, 279–290. (In Chinese)
60. Chi, X.G.; Dong, C.Y.; Liu, J.F.; Jin, W.; Li, C.; Liu, S.; Li, G.R. High Mg[#] low Mg[#] potassic-ultrapotassic volcanic rocks and their source nature on the Tibetan Plateau. *Acta Petrol. Sin.* **2006**, *22*, 595–602. (In Chinese)
61. Becker, G.F. Fractional crystallization of rocks. *Am. J. Sci.* **1897**, *4*, 257–261. [[CrossRef](#)]
62. Hildreth, W. Volcanological perspectives on Long Valley, Mammoth Mountain, and Mono Craters: Several contiguous but discrete systems. *J. Volcanol. Geotherm. Res.* **2004**, *136*, 169–198. [[CrossRef](#)]
63. Taylor, S.R.; Heier, K.S. The petrological significance of trace element variations in alkali feldspars. *Proc. XXI Int. Geol. Congr.* **1960**, *14*, 47–61.
64. Heier, K.S.; Taylor, S.R. Distribution of Li, Na, K, Rb, Cs, Pb and Tl in southern Norwegian pre-cambrian alkali feldspars. *Geochim. Cosmochim. Acta* **1959**, *15*, 284–304. [[CrossRef](#)]

Disclaimer/Publisher's Note: The statements, opinions and data contained in all publications are solely those of the individual author(s) and contributor(s) and not of MDPI and/or the editor(s). MDPI and/or the editor(s) disclaim responsibility for any injury to people or property resulting from any ideas, methods, instructions or products referred to in the content.